THE JOURNAL OF PHYSICAL CHEMISTRY B

Article

pubs.acs.org/JPCB

Block Copolymer Micelles as Nanoreactors for Self-Assembled Morphologies of Gold Nanoparticles

Poonam Khullar,[§] Vijender Singh,[§] Aabroo Mahal,[§,∥] Harsh Kumar,[∥] Gurinder Kaur,[‡] and Mandeep Singh Bakshi*[,†]

[†]Department of Chemistry, Wilfrid Laurier University, Science Building, 75 University Ave. W., Waterloo ON N2L 3C5, Canada

[‡]Nanotechnology Research Laboratory, College of North Atlantic, Labrador City, NL A2 V 2K7 Canada

[§]Department of Chemistry, B.B.K. D.A.V. College for Women, Amritsar 143005, Punjab, India

[∥]Department of Chemistry, Dr. B. R. Ambedkar National Institute of Technology, Jalandhar-144011, India

Supporting Information

ABSTRACT: Self-assembled gold (Au) nanoparticles (NPs) were synthesized in micelle surface cavities of a L121 block polymer in the presence of zwitterionic (viz. DPS, TPS, and HPS) and sugar surfactants (OG and DDM) in aqueous phase at 70 °C by using the surface cavities of L121 as reducing sites for converting Au(III) into Au(0). All reactions were monitored simultaneously by UV−visible spectroscopy to determine the growth kinetics in gold nucleating centers on the basis of surface plasmon resonance that also helped in tracing the structure micelle transitions over a wide temperature range of 10−70 °C. The surfactant/L121 mole ratio was changed systematically from 0.5 to 2.5 by keeping L121 and $HAuCl_4$ concentrations constant at 10 and 0.25 mM, respectively, to determine the shape and size of the micelles and their relation to the self-assembled behavior of Au NPs. TEM studies were used to have a direct insight into the morphology of micelle templates and their shape and size for self-assembled NPs. L121 along with DPS (C12 carbon chain) produced well-defined micelles loaded with tiny NPs of 3−6 nm in the L121-rich region of the mixture, while large flower-like compound micelles with a clear core−shell morphology were produced in the DPS-rich region. TPS and HPS (C14 and C16 hydrocarbon chains, respectively) with stronger hydrophobicity than DPS also produced almost similar micelles loaded with tiny NPs in the L121-rich region, but they disappear in the surfactant-rich region. Replacement of zwitterionic with ionic surfactants did not yield micelle templates for self-assembled NPs. Results conclude that well-defined micelles of L121 are the fine templates for self-assembled NPs that can only be achieved in the presence of a neutral surfactant with low concentration and low hydrophobicity.

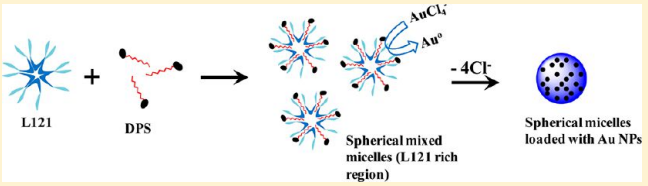

INTRODUCTION

Polyethylene−polypropylene−polyethylene (PEO−PPO−PEO) triblock polymers (TBPs) are water-soluble polymeric surfactants with unique micelle properties[1−4] that are dramatically influenced by the concentration as well as temperature (viz. critical micelle temperature, cmt;[5] critical micelle concentration, cmc;[6−11] and cloud point, cp). A typical TBP micelle consists of predominantly hydrophobic PPO blocks as the core and hydrophilic PEO blocks as the shell with a variable degree of aggregation numbers due to inherent polydipersity.[5,6] TBP micelles are usually much larger in size than the conventional surfactant micelles, and their size ranges from about 50 nm to more than 200 nm and is generally related to the average molar mass of the polymer.[4] Such large micelles are fine templates for accommodating small Au NPs. Direct visualization of such assemblies by imaging techniques is a challenging task because usually surfactant micelles exist in dynamic equilibrium in the aqueous phase. However, if suitable conditions are created so as to make them predominantly hydrophobic, it is possible to extract them in the dried state for direct visualization. Direct visualization of the micelle assemblies provides far more information than by any indirect solution technique. We are reporting a simple procedure that allows us to extract micelles loaded with tiny Au NPs in the dried state and characterize them directly. It further helps us to even closely monitor the structure transitions leading to different morphologies, which are otherwise a tedious task to analyze through conventional solution phase techniques. It can simply be achieved by choosing predominantly hydrophobic micelles, as in L121, PEO_5−PPO_{68}−PEO_5. Unlike conventional surfactant micelles, the presence of ether oxygens in the TBP micelle core does not allow it to attain a complete hydrophobic environment. A larger PEO block allows micelles to attain greater hydration and vice versa, but a larger PPO block (as in L121) renders TBP water insoluble due to a predominant hydrophobicity. Such a TBP can be made water-soluble if sufficient hydrophilicity is introduced by allowing the ether oxygens to get hydrated, and that can be done by incorporating

Received: October 23, 2012
Revised: January 21, 2013
Published: March 4, 2013

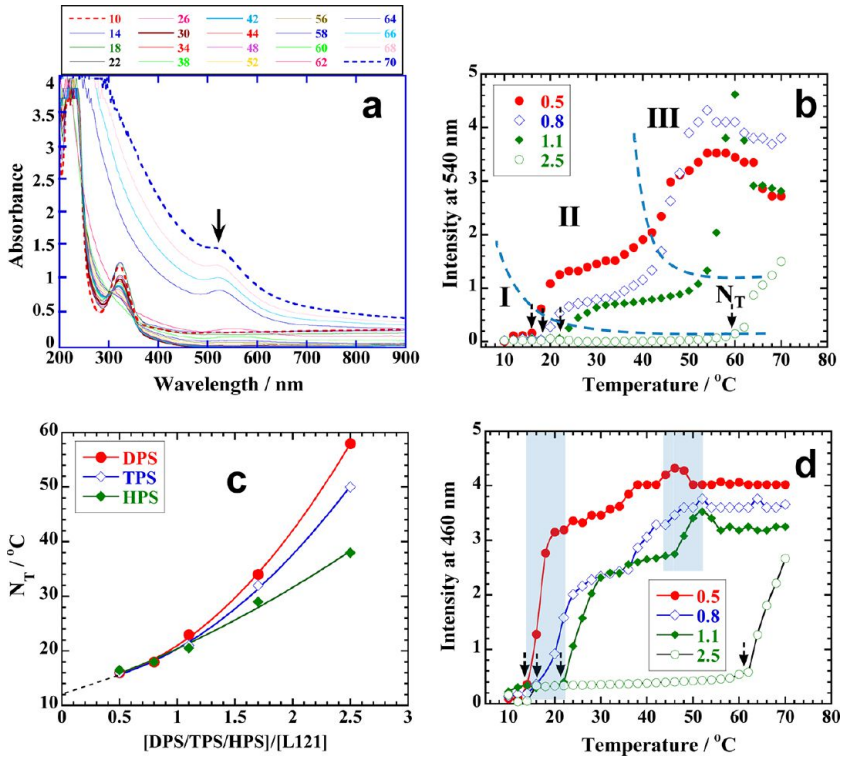

Figure 1. (a) Plot of absorbance versus wavelength for DPS + L121 + $HAuCl_4$ with DPS/L121 mole ratio = 2.5 at different temperatures from 10–70 °C. Black arrow indicates the absorbance due to surface plasmon resonance of Au NPs. (b) Intensity versus temperature plot for different mole ratios of DPS/L121. Dotted arrows indicate the nucleation temperature (N_T). (c) Plot of N_T versus surfactant/L121 mole ratios for DPS, TPS, and HPS. (d) Intensity versus temperature plot of MO at different mole ratios of DPS/L121. See details in the text.

conventional surfactant monomers to generate mixed micelles.[12−19] The mixed micelles thus created are expected to be well-defined and relatively less polydisperse due to their predominant hydrophobic nature and hence are versatile micelle templates for accommodating Au NPs. The best way to bring and accommodate Au NPs on micelle templates is to simultaneously synthesize them by using their surface cavities lined with reducing ether oxygens.[20−27] In this way, Au NPs are synthesized from the nucleating centers, and immediately accommodated in the surface cavities in the form of a self-assembled arrangement.

Micelle stability is the most important factor to attain the self-assembled arrangement of NPs on the micelle surface because a stable micelle has a proper arrangement of surface cavities, which are the reaction sites for the conversion of Au (III) into Au (0). Predominantly hydrophilic micelles with greater hydration are prone to self-association and form compound micelles with no clear surface arrangement of surface cavities; therefore, predominantly hydrophobic micelles are always good templates.[28−32] Since the reduction of Au(III) into Au(0) is facilitated in the aqueous phase, therefore, the stability of predominantly hydrophobic micelles, as in L121, in the aqueous phase can be achieved only by incorporating the surfactant monomers, which impart required hydration to the stern layer (i.e., shell of TBP micelle).[6−11] Surfactants of different polarities in the mixed state with L121 can have a dramatic influence on the synthesis of Au NPs by modifying the surface arrangement of PEO surface cavities. Addition of ionic surfactants, such as sodium dodecyl sulfate (SDS) and cetyltrimethyl ammonium chloride (CTAC), to a relatively less hydrophobic P123 disrupts the polymer aggregates and induces significant hydration in the PPO block.[18] Both surfactants form a liquid crystalline phase with L121 and dismantle the polymer aggregates with a predominate effect demonstrated by CTAC than SDS.[17,18] Low concentrations of ionic surfactants mainly form polymer-rich mixed micelles, whereas intermediate concentrations simultaneously produce small surfactant-rich aggregates.[17] Similar interactions are observed with nonionic surfactants, but with a relatively lesser magnitude than ionic surfactants based upon the regular solution approximations.[19] Therefore, the choice of an appropriate surfactant is an important aspect to be taken in consideration to obtain suitable micelle templates for Au NPs.

Our aim in this work is to analyze different surfactant−L121 systems for their suitability to accommodate Au NPs on the micelle templates in terms of micelle shape and size under the effect of temperature and concentration. We want to demonstrate these findings in one of the simplest ways of imaging studies of direct visualization of such morphologies. Self-assembled NPs help us to achieve this objective due to their strong contrast against otherwise transparent micelles by using TEM. Direct imaging is only achieved in the dried state where stability of the micelle template matters. Thus, predominantly hydrophobic micelles are required as micelle templates so that they could be created in the aqueous phase, but visualized in the dried state. This allows us to characterize such complex aggregated assemblies as far as their size, shape, and transitions are concerned. These characteristic features are important in view of their significant implications as nanoreactors,[33−35] biosensors, biolabeling agents, and agents for diagnostic assay.[36−39]

dx.doi.org/10.1021/jp310507m | J. Phys. Chem. B 2013, 117, 3028−3039

EXPERIMENTAL SECTION

Materials. Chloroauric acid ($HAuCl_4$), triblock polymer L121 ($PEO_5-PPO_{68}-PEO_5$), sodium dodecyl sulfate (SDS), sodium perfluorooctanoate (SPO), octyl β-D glucopyranoside (OG), and *n*-dodecyl β-D maltoside (DDM) were purchased from Sigma-Alrdich. 3-(*N*,*N*-Dimethyldodecyl ammoniopropane sulfonate) (DPS), 3-(*N*,*N*-dimethyltetradecyl ammoniopropane sulfonate) (TPS), and 3-(*N*,*N*-dimethylhexadecyl ammoniopropane sulfonate) (HPS, 98%) were obtained from Fluka. Double distilled water was used for all preparations.

Synthesis of Au NPs. Aqueous mixtures (total 10 mL) of L121 (10 mM), surfactant (5−25 mM), and $HAuCl_4$ (0.25 mM) were taken in screw-capped glass bottles. After mixing the components at room temperature, the reaction mixtures were kept in a water thermostat bath (Julabo F25) at a precise temperature of 70 ± 0.1 °C for 6 hours under static conditions. The color of the solution changed from colorless to pink-purple or purple with the passage of time and remained the same thereafter in most of the cases. Some of the reactions produced colored gel (Supporting Information, Figure S1). After 6 hours, the samples were cooled to room temperature and kept for overnight. They were purified from pure water at least two times in order to remove unreacted TBP/surfactant. Purification was done by collecting the Au NPs at 10 000−12 000 rpm for 5 min after washing each time with distilled water. These samples were used for TEM analysis.

Methods. To understand the reaction kinetics of the synthesis of Au NPs, each reaction was monitored by simultaneous UV−visible measurements with the temperature between the temperature range of 10−70 °C to determine the influence of micelle transitions on the synthesis of Au NPs. All reactions were performed in the UV cuvette with the help of a Shimadzu model No. 2450 (double beam). This instrument is equipped with a TCC 240A thermoelectrically temperature-controlled cell holder that allows measuring the spectrum at a constant temperature within ±1 °C. Control experiments were carried out with 25 μM methyl orange (MO) in the temperature range of 10−70 °C to determine the micelle structure transitions. The intensity at 460 nm of MO versus temperature plot gives a sigmoidal curve that indicates the micelle transition with an estimated error of ±5%.

Transmission electron microscopic (TEM) analysis was done on a JEOL 2010F at an operating voltage of 200 kV. The samples were prepared by mounting a drop of a solution on a carbon-coated Cu grid and allowed to dry in the air.

RESULTS

UV−Visible Studies. *Nucleation.* Reaction kinetics of all reactions was simultaneously monitored by UV−visible measurements on the basis of the SPR of growing nucleating centers within the temperature range of 10−70 °C. Figure 1a shows a typical reaction for DPS/L121 mole ratio = 2.5 in the presence of 0.25 mM $HAuCl_4$. A systematic temperature variation from 10 to 70 °C progressively converts Au(III) into the Au(I) transition state in the form of a ligand-to-metal charge-transfer band (LMCT)[26] around 320 nm that subsequently converts into Au(0) to start nucleation. Absorbance around 540 nm is due to the SPR of growing Au nucleating centers,[40,41] and its variation is depicted in Figure 1b for different DPS/L121 mole ratios. For a mole ratio of 2.5, a practically insignificant absorbance is observed till 62 °C, where the LMCT complex disappears and converts into small nucleating centers that subsequently grow into NPs with significant absorbance.[26,27] We designate 62 °C as the nucleating temperature (N_T, indicated by dotted arrows in each case) where LMCT attains sufficient energy and converts into nucleating centers. A similar trend is observed at lower mole ratios, and N_T decreases with the decrease in the mole ratio or decrease in the amount of DPS. Its nonlinear variation with mole ratio is shown in Figure 1c. LMCT is mainly initiated due to the charge donation from predominantly ligand $3e_u(\pi)$ electron-rich ether oxygens of PEO or PPO blocks to electron-deficient metal $3b_{1g}(\sigma^*)$ molecular orbitals of $AuCl_4^-$ ions when ions are accommodated in the micelle surface cavities.[26] A higher amount of DPS (mole ratio = 2.5) disturbs this arrangement to a greater extent than a lower amount (mole ratio = 0.5) and thus generates a weaker LMCT complex in the former case that requires high temperature (N_T = 62 °C) to convert into nucleating centers. Furthermore, as the hydrophobicity increases from DPS to HPS, its LMCT destabilizing effect reduces because HPS−L121 mixed micelles attain higher hydrophobicity with a relatively compact arrangement of surface cavities. This reduces the N_T systematically in the order of DPS > TPS > HPS (Figure 1c). All curves merge with each other at low mole ratios and extrapolate to 10 °C in the absence of surfactant, which means that L121 is capable of generating nucleating centers as soon as $AuCl_4^-$ ions are accommodated in the surface cavities without going through LMCT. Thus, stronger reducing conditions (i.e., low mole ratio) converts Au(III) into Au(0) at relatively lower temperatures than the weaker reducing conditions (i.e., high mole ratio).

Growth. Growth of the nucleating centers created after N_T in each case shows some interesting variation especially for the low mole ratios (Figure 1b). For a better understanding, we have illustrated Figure 1b in the form of a phase diagram with different regions. Part I of the phase diagram depicts the region where only the LMCT complex exists; hence no absorbance due to SPR of NPs is observed. This region dramatically shrinks to low temperature with a decrease in the mole ratio, which indicates that the low mole ratio does not promote the LMCT complex formation. Part II starts soon after the formation of nucleating centers and depicts their growth with temperature. As nucleating centers convert into tiny NPs, their absorbance shows a sudden increase initially, but remains weak thereafter over a wide temperature range. It means that, once the NPs are created after N_T, they do not show any substantial growth over a wide temperature range of this region. As the temperature reaches the part III, a dramatic rise in the intensity, indicating a substantial growth in the number density of NPs, is observed. To understand this behavior, we carried out parallel control experiments in the absence of $HAuCl_4$ and in the presence of MO dye to follow the micelle structure transitions with temperature. It should be mentioned that micelle structure transitions have a dramatic effect on the arrangement of surface cavities that control the reduction of Au(III) into Au(0).[26,27] MO is expected to solubilize in the palisade layer predominantly occupied by the PPO blocks at the interface of the core and shell of the micelle due to the phenyldiazenyl group. As the micelle gets dehydrated with temperature, MO releases in the aqueous phase. As a result, its intensity increases. Therefore, a sudden change in the intensity of MO in fact refers to the ongoing micelle transitions with temperature. It is interesting to note that the variation in the intensity of MO at 460 nm

dx.doi.org/10.1021/jp310507m | J. Phys. Chem. B 2013, 117, 3028−3039

(Figure 1d) follows an almost identical behavior to that of Figure 1b, suggesting the fact that the growth of the NPs in Figure 1b is entirely controlled by the micelle transitions. In addition, N_T (Figure 1b) corresponds to the release of MO from the micellar phase in each case (see dotted arrows, Figure 1d). It means that the conversion of LMCT into nucleating centers happens during the first micelle transition (left band for low mole ratios, Figure 1d). It is thus driven by a rapid dehydration of PPO rather than the PEO block of the micelles due to the greater tendency of the PPO block to lose water at low temperature. Dehydration increases the hydrophobicity and makes micelles more compact and hence provides a compact arrangement to surface cavities. A compact arrangement enhances their electron-donating ability and hence provides sufficient energy to convert LMCT into nucleating centers (or, in other words, to convert Au(III) into Au(0)) that subsequently grow into tiny NPs.[26] Since after this, there is no dramatic change in the release of MO (Figure 1d) over a wide temperature range, therefore, no appreciable growth in the NPs is also observed (part II of Figure 1b). It means that the micelles remain energetically stable[42,43] over a wide temperature range before they undergo a second transition (right band, Figure 1d), which corresponds to part III of the phase diagram (Figure 1b). A much weaker rise in the intensity of MO (Figure 1d) in this region further confirms its preferential solubilization in the palisade layer close to the core of the micelle rather than in the shell constituted by the PEO blocks. That is why dehydration due to the second transition releases a little amount of MO while it induces a significant growth in the NPs because the dehydration of the shell (PEO blocks) further squeezes the surface cavities already carrying tiny NPs to a greater extent. This facilitates the interparticle fusion among the tiny NPs to further grow in their size with enhanced SPR.[44,45] It also results in the subsequent gel formation with entrapped NPs (Figure S1, Supporting Information) and consequently causes a decrease in the intensity thereafter. Therefore, the first transition is mainly related to the dehydration of PPO blocks and is responsible for the formation of nucleation centers, whereas the second transition contributes toward the growth of the NPs.

Influence of Surfactant Headgroup. The above discussion clearly indicates the marked effect of zwitterionic surfactant on the overall physiochemical behavior of L121 micelles and their subsequent effect on the growth kinetics of Au NPs. Figure 2 compares this effect for surfactants of different categories at a constant surfactant/L121 mole ratio of 0.5. Replacing the zwitterionic headgroup of DPS with sugar, as in the case of DDM, initiates the formation of nucleating centers at the same temperature with an almost similar variation in the absorbance of growing NPs. A neutral nature of DDM, like that of DPS, seems to be the reason behind this. Although, the anionic surfactant SDS also starts the formation of nucleating centers at the same temperature, NPs grow instantaneously with a rapid growth initially and then their growth becomes constant soon after with no sign of a second transition. It means that the addition of SDS completely breaks down the L121 micelles immediately after the first transition and simultaneously generates small mixed micelles with little participation in the growth kinetics of the NPs.[17,18] This was not the case with either DPS or DDM in view of their neutral natures. To ascertain this further, we selected SPFO, another anionic surfactant with much enhanced hydrophobicity due to the fluorocarbon chain, so that the hydrophobic environment could be strengthened in order to allow the participation of surface cavities in the growth process. However, the behavior of SPFO remains the same to that of SDS, which means that both anionic surfactants dismantle the large L121 micelles to produce small mixed micelles that are unable to control the growth of Au NPs.

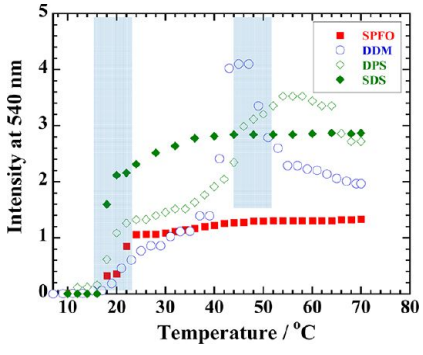

Figure 2. Plot of absorbance versus wavelength for surfactant + L121 + $HAuCl_4$ with surfactant/L121 mole ratio = 0.5 at different temperatures from 10 to 70 °C. See details in the text.

Now we need to rationalize the results of Figures 1 and 2 on the existence of micelle templates because they are primarily responsible for the self-assembled NPs. A qualitative analysis of Figure 2 suggests that the micelle templates are present in those surfactant + L121 mixtures in which micelle structure transitions of L121 micelles control the growth of NPs due to the presence of surface cavities. The surface cavities not only are involved in the reduction process but also accommodate the resulting NPs on micelle templates. This is happening in the case of DPS and DDM, where micelles survive over a wide temperature range (~10−60 °C) and is evident from the ongoing growth process. However, the absence of the growth process in the presence of SDS and SPFO indicates the absence of surface cavities and obviously of micelle templates due to enhanced electrostatic interactions in the shell, which carries surface cavities. Direct imaging studies, such as TEM analysis, of the micelles carrying self-assembled Au NPs can help us to authenticate these observations.

Microscopic Studies. *L121 + DPS Mixtures.* We have performed a systematic TEM analysis of various samples of different mole ratios to understand the shape and size of micelle templates carrying Au NPs. Figure 3a shows a low-magnification TEM image of a sample prepared with DPS/L121 mole ratio = 0.5. This sample on a copper grid shows several dark dots, and some of them are indicated by dotted circles. These dots are, in fact, micelles carrying self-assembled NPs, as evident from a high-resolution image (Figure 3b). Each micelle carries several small NPs of 2−4 nm. Some micelles also show even slightly bigger fused NPs of 6−7 nm (indicated by white arrows in Figure 3c), which might be produced due to interparticle fusion during a substantial growth, as depicted in Figure 1b. All micelles (Figure 3a−c) are well-defined roughly spherical, and NPs are uniformly distributed among them with no sign of their independent existence. It supports our previous observations (Figure 1b) that NPs only grow on micelle templates through the reduction reaction conducted by the micelle surface cavities[20−22,26,27] and micelles are sufficiently hydrophobic; that is why they survive in the dried state. An increase in the mole ratio from 0.5 to 0.8 produces similar well-defined micelles (Figure 3d). Some of the micelles are attached

dx.doi.org/10.1021/jp310507m | J. Phys. Chem. B 2013, 117, 3028−3039

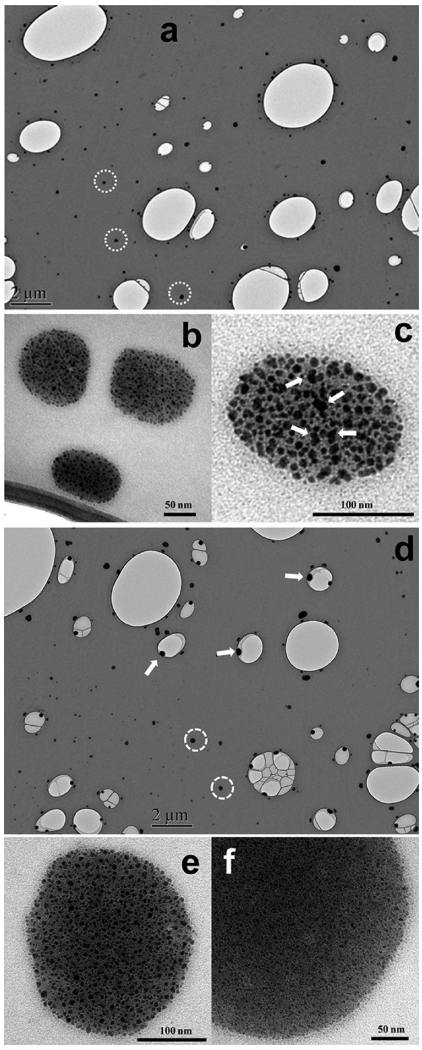

Figure 3. (a) Low-resolution TEM image of a sample prepared with DPS/L121 mole ratio = 0.5 at 70 °C. Dotted white circles enclose single micelles. (b, c) High resolution images of different roughly spherical micelles with self-assembled Au NPs of 2−6 nm in size. White arrows in (c) indicate some fused NPs. (d) Low-resolution TEM image of a sample prepared with DPS/L121 mole ratio = 0.8 at 70 °C. Again, dotted white circles enclose single micelles. (b, c) High-resolution images of a single micelle with self-assembled NPs. See details in the text.

to the inner walls of the empty vesicles (indicated by white arrows). Each micelle contains uniformly distributed Au NPs of 2−4 nm (Figure 3e). NPs are thoroughly embedded in the micelles, as evident from the high-magnification image (Figure 3f). Practically no marked difference is observed between the micelle templates of mole ratios of 0.5 (Figure 3a−c) and 0.8 (Figure 3d−f) as far as their micelle shapes are concerned, whereas variable sizes are obviously due to their inherent polydisperse behavior. Micelle transitions as well as growth kinetics depicted by UV−visible behavior (Figure 1b) for both mole ratios are quite similar, and hence, obviously similar micelle morphologies are expected.

As the amount of DPS increases further in the mole ratio of 1.1, dramatic changes in the shape and size of the micelles are observed. This is the first time many compound micelles are present (indicated by white arrows in Figure 4a) apart from the regular micelles. A magnified view of such a compound micelle

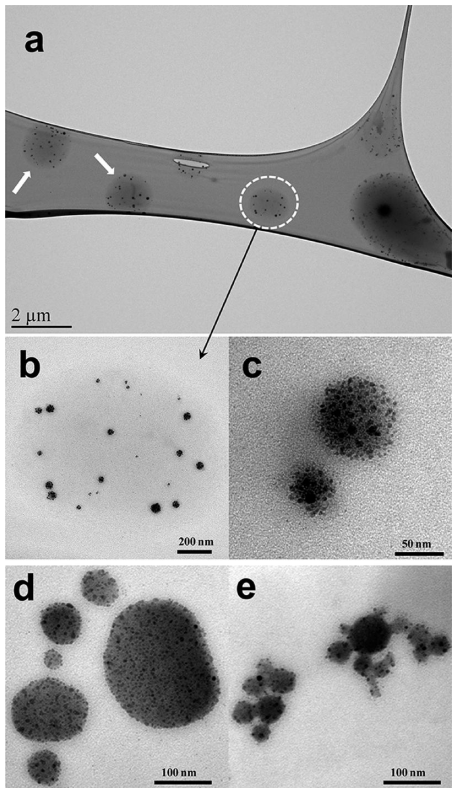

Figure 4. (a) Large diluted micelles of a sample prepared with DPS/L121 mole ratio = 1.1. High-resolution images are shown in (b, c). (d, e) High-resolution TEM images of micelles of different sizes along with subdivided micelles bearing small NPs. See details in the text.

is shown in Figure 4b. This micelle contains further small micelles (Figure 4c) that act as templates for self-assembled tiny NPs. Compound micelles are the consequence of increased hydration of the L121 micelles in view of the greater amount of DPS, which makes a micelle less hydrophobic and less well-defined and hence tends to break into the smaller ones with predominantly hydrophobic domains. Eisenberg et al[29,46] previously reported polystyrene-*b*-poly(acrylic acid) compound micelles produced from reversed micelles by changing the solubility of the corona and core components due to the solvent. In addition to the compound micelles, regular micelles show a high tendency to break into smaller ones (Figure 4d,e). Again, this is happening due to greater hydration, which does not allow the larger micelle to be held by the weakening hydrophobic environment. Smaller micelles are also templates for self-assembled NPs. Thus, the induced hydration causes a marked shift in the N_T as well as in the subsequent growth process toward higher temperatures for this mole ratio in Figure 1b, because higher temperature is required to increase the reduction potential of surface cavities by bringing them closer.[26,27] Close inspection of Figure 1b shows an extended part II region for the mole ratio of 1.1 in comparison to 0.5 and 0.8 due to a greater amount of hydration that requires higher temperature for the second transition.

A further increase in the mole ratio to 2.5 significantly increases the amount of DPS than L121. This causes the formation of unique morphologies (Figure 5a) that are much different from the typical micelles produced at lower mole ratios. They are monodisperse, roughly spherical flower-like, and much larger in size (∼1 μm), and they mostly exist in the form of small aggregates of two to four micelles (Figure 5b).

dx.doi.org/10.1021/jp310507m | *J. Phys. Chem. B* 2013, 117, 3028−3039

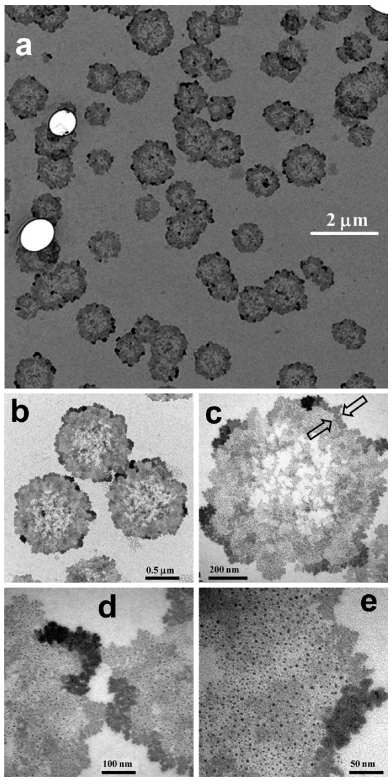

Figure 5. (a) Low-resolution TEM image of flower-like large compound micelles prepared with DPS/L121 mole ratio = 2.5. (b–e) High-resolution images of the same sample with different magnifications showing a core–shell morphology as well as tiny Au NPs. See details in the text.

Each morphology is made up of a less-dense large core and a relatively more compact thin shell of ~50 nm (Figure 5c). They are interconnected with each other through the overlapping of the thin shells of adjoining micelles (Figure 5d). Surprisingly, now the large core predominantly contains a significantly higher number density of 2–3 nm Au NPs than the shell (Figure 5e). This arrangement of tiny NPs seems to be opposite to what we have observed for the micelle templates of lower mole ratios where the amount of L121 was higher than that of DPS. A much larger amount of DPS has the ability to solubilize the predominantly hydrophobic PPO block of L121 in its micelles. The PPO block of L121 contains 58 PO units that are not supposed to be solubilized in a relatively much smaller micelle of DPS. Thus, solubilization is simultaneously facilitated by several DPS micelles, resulting in the formation of a compound micelle[29,46] (Figure 5c), which accommodates mainly L121 in a large, less-dense core while predominantly hydrophilic DPS constitutes the shell. This arrangement pushes the surface cavities in the anterior of the compound micelle, and that is why a greater number density of tiny NPs is found in the core rather than in the shell (Figure 5e). Furthermore, the larger amount of DPS highly hydrates the core, and hence, in the dried state, it seems empty with fragments of L121 (Figure 5c). Such a compound micelle obviously needs 62 °C to initiate the nucleation (Figure 1b), in contrast to the lower mole ratios (~20 °C).

L121 + TPS/HPS Mixtures. With a mole ratio of 0.5, L121 along with TPS produces similar micelle templates loaded with NPs of 2–3 nm. Almost all micelles are attached to either the outer or the inner walls of the empty vesicles (see empty white block arrows in Figure 6a) and tend to attain the shape of the portion of the vesicle. For instance, Figure 6b,c shows rectangular and hemispherical micelles, respectively, thoroughly loaded with tiny NPs because they happen to be there where they can attain such shapes. An oval-shaped micelle (Figure 6d) probably is obtained from the bifurcation of the elongated micelle (Figure 6e). Choosing HPS instead of TPS shows micelles of various shapes (Figure 6f), again entrapped in empty vesicles, which are now nonspherical with nonuniform distributions of NPs throughout the micelle. For instance, see the micelles of Figure 6g,h, where white block arrows indicate relatively larger NPs accumulated at the periphery. There are many long, rod-shaped micelles as well (Figure 6i), which we do not observe in the presence of either DPS or TPS. This sequence of different micelle templates demonstrates a high degree of micelle transitions from sphere to rod, which is governed by the increasing hydrophobicity in the order of DPS < TPS < HPS. A further increase in the amount of TPS with a mole ratio of 0.8 generates distorted micelles of variable shapes and sizes containing Au NPs (Figure 7a–c), contrary to the well-defined micelles produced at 0.5 (Figure 6a–e). They look as if they are diluting away. HPS, on the other hand, produces roughly spherical large micelle templates (Figure 7d). Some micelles are close to 1 μm and thoroughly loaded with tiny NPs (Figure 7e). Interestingly, some of the large micelles now carry large interconnected NPs (Figure 7f,g) that might have been produced from the interparticle fusion[44,45] of the tiny NPs that initiated at 0.5 (Figure 6g,h). Other morphologies of different shapes (Figure 7h) also exist, as observed for 0.5. Thus, a slight increase in the amount of TPS and HPS from a 0.5 to 0.8 mole ratio brings some visible changes in the shape and size of the micelle templates, contrary to quite similar morphologies of both mole ratios for DPS (Figure 3). Clearly, enhanced hydrophobicity affects the morphologies of micelle templates, thus making them more prone to structure transitions.

However, a further increase in the mole ratio to 1.1 (Figure S2, Supporting Information) and 2.5 (Figure S3, Supporting Information) for both surfactants does not yield any micelle templates, instead predominantly platelike[47] triangular and hexagonal NPs along with other smaller shapes are produced for TPS (Figure 8a,b) as well as HPS (Figure 8c,d) mixtures with L121. Each platelike morphology (Figure 8e) is single-crystal with a hexagonal atomic arrangement (Figure 8f) and predominant growth along the {111} crystal planes. This seems to be quite contrary to their UV–visible behavior, which clearly shows the growth process controlled by the micelle transitions (Figures S4 and S5, Supporting Information, respectively), just like that of DPS mixtures (Figure 1b). It means that the micelles are primarily responsible for the growth of NPs but unable to carry them as templates. This could be due to the following reasons: First, NPs are too big (nanoplates ≈ 100 nm in comparison to 2–4 nm tiny NPs) to be accommodated on micelle templates. Second, TPS already induced the micelle deformation at 0.8 (Figure 7a–c) due to its enhanced solubilization effects. Therefore, a mole ratio of 1.1 is not expected to have similar micelle templates with a greater amount of TPS than L121. The same situation happens for HPS where bigger NPs have already started forming at a mole ratio of 0.8 (Figure 7f,g), and hence, a mole ratio of 1.1 is expected to facilitate this process. Thus, breakdown of the large micelle templates into surfactant-rich small mixed micelles takes place[17–19] at a mole ratio of 1.1, and hence, no more templates are formed. This shows that the micelle templates exist only in

dx.doi.org/10.1021/jp310507m | J. Phys. Chem. B 2013, 117, 3028–3039

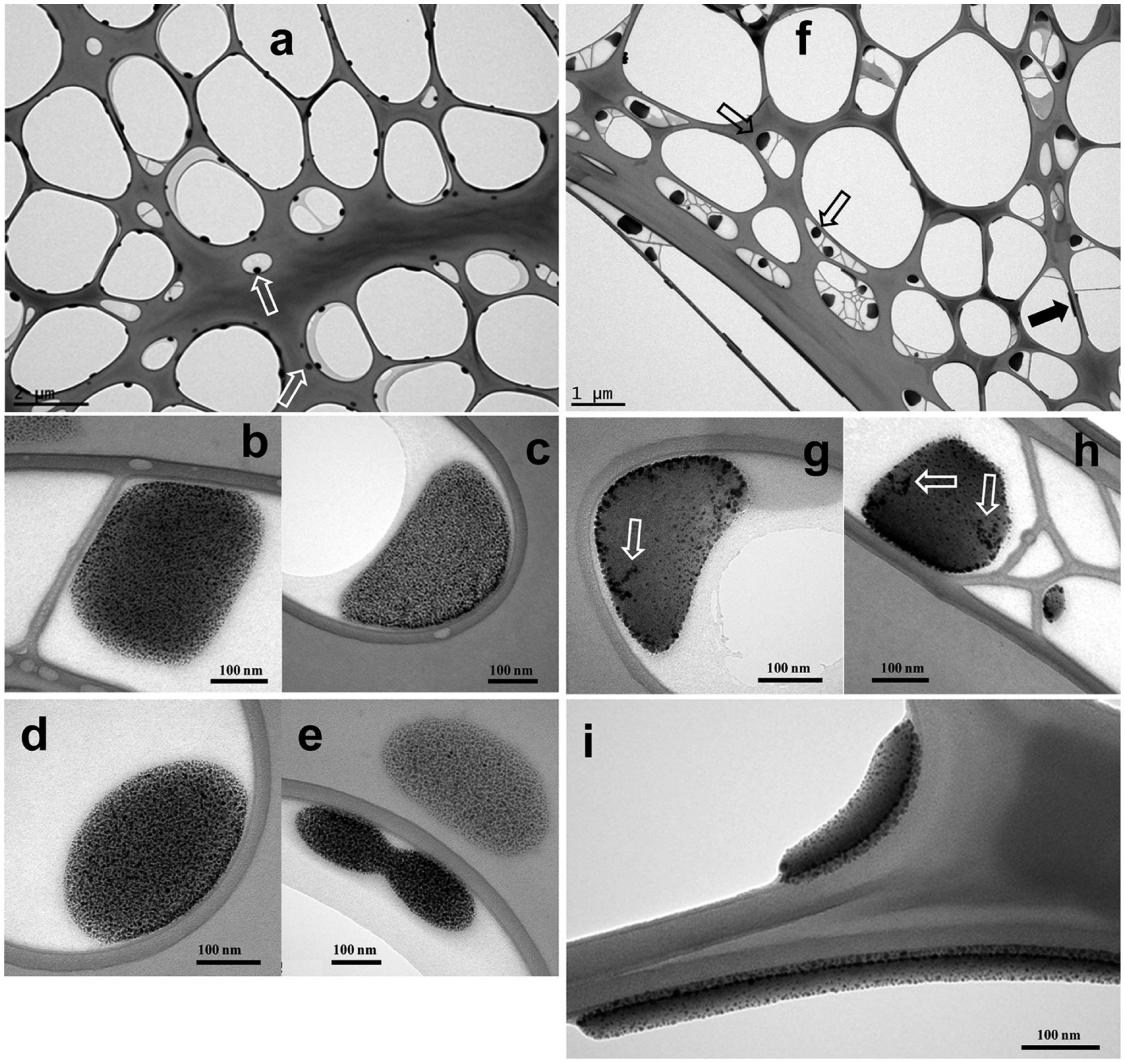

Figure 6. (a) Low-resolution TEM image of a sample with TPS/L121 mole ratio = 0.5. White block arrows indicate the locations of different micelles inside the large empty vesicles. (b–e) High-resolution images of different shapes of micelles bearing tiny NPs of 2–3 nm in size. (f) Low-resolution image of a sample with HPS/L121 mole ratio = 0.5. Empty block arrows indicate the presence of several entrapped micelles in empty vesicles, whereas the filled block arrow indicates a long, rod-shaped micelle. (g, h) High-resolution TEM image of different micelles in which white block arrows indicate the strands of fused NPs. (i) Similar image of long, rod-shaped micelles bearing tiny NPs. See details in the text.

low mole ratio mixtures where the amount of L121 is appreciably higher than that of highly hydrophobic surfactants (i.e., TPS and HPS).

L121 + OG/DDM Mixtures. Figure 9a,b depicts the micelle templates of L121 + OG and L121 + DDM mixtures with a mole ratio of 0.5. Both images show large micelle templates carrying tiny NPs of 2–4 nm. A single spherical micelle loaded with such NPs is shown in Figure 9c, while Figure 9d shows a high-resolution image. Each tiny NP is single-crystal with a lattice spacing of 0.20 nm that originates from the {200} reflection of fcc gold (Figure 9e). It further supports our earlier conclusions drawn from Figure 2 that neutral surfactants are the most appropriate choice for the micelle templates to accommodate Au NPs. In contrast, the additive effect of SDS (no micelle templates, Figure S6, Supporting Information) and SPFO (no micelle templates, Figure S7, Supporting Information) is so strong that even a 0.5 mole ratio completely eliminates the micelles.[48,49] This is previously depicted in Figure 2, where the growth process of NPs for the L121 + SDS/SPFO mixtures does not show any micelle transitions, and consequently, no micelle templates are formed. Therefore, low amounts as well as low hydrophobicity of a neutral surfactant are the important parameters that favor the stability of the micelle templates in aqueous phase. On the other hand, an even higher hydrophobicity that facilitates the solubilization of PPO/PEO blocks and the polarity of a surfactant also destabilize and break down the micelle templates, which consequently eliminate the self-assembled arrangement of NPs, and that is why we do not see micelle templates in the case of SDS and SPFO mixtures with L121.

■ DISCUSSION

All results have been summarized in a phase diagram (Figure 10) that depicts the variation of shape and size of the micelle templates with mole fraction as well as hydrophobicity of the zwitterionic surfactant and are schematically represented in Figure 11. This phase diagram (Figure 10) has been divided into TBP and surfactant-rich regions. Large micelle templates of different shapes and sizes loaded with self-assembled NPs are mainly present in the TBP-rich region. L121 with DPS (C12)

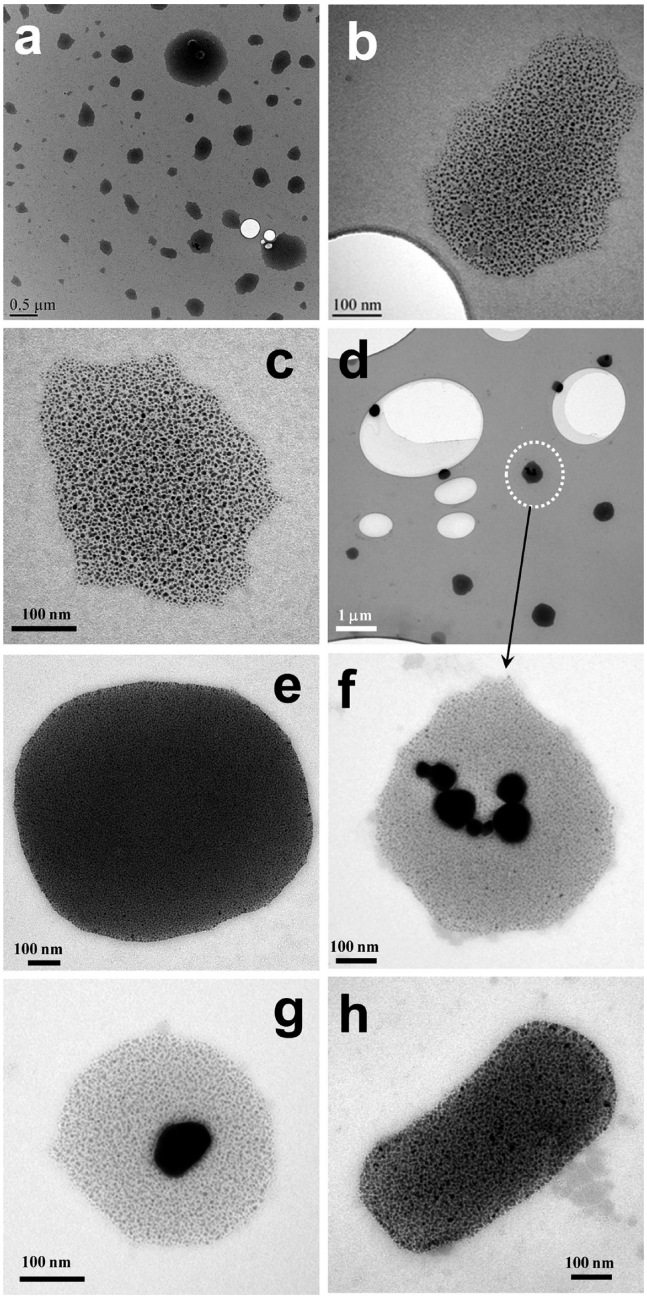

Figure 7. (a–c) Low- and high-resolution images, respectively, of a sample prepared with TPS/L121 mole ratio = 0.8 showing large distorted micelles loaded with tiny NPs. (d) Low-resolution image of a sample prepared with HPS/L121 mole ratio = 0.8. (e) A large micrometer-sized micelle loaded with tiny NPs. Panels (f) and (g) show micelles containing large fused and single Au NPs along with tiny NPs. Panel (h) shows a rod-shaped micelle. See details in the text.

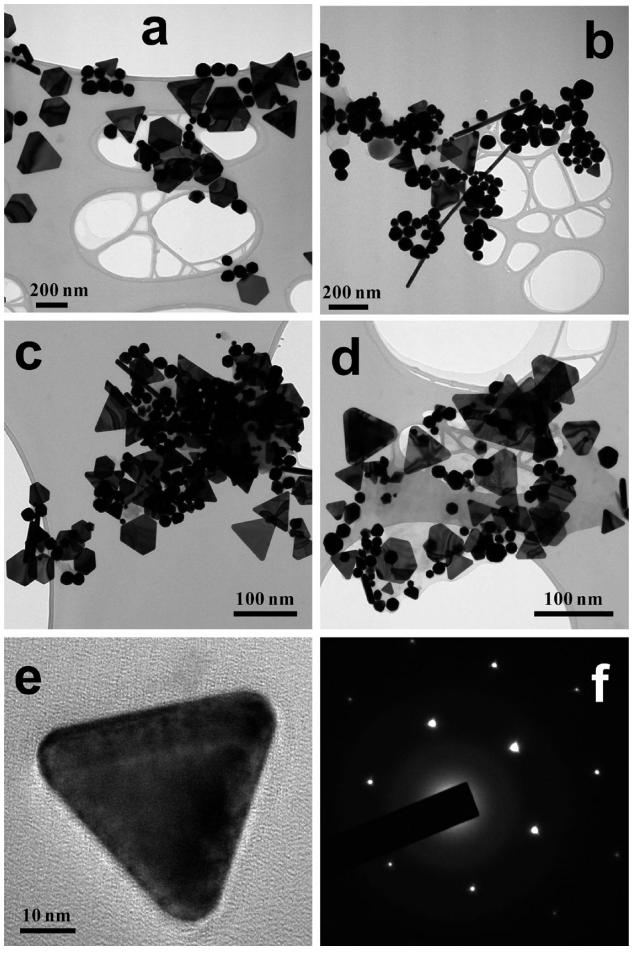

Figure 8. (a,b) TEM images of a sample prepared with TPS/L121 mole ratio = 1.1 and 2.5, respectively. (c, d) Similar images with HPS/L121 mole ratio = 1.1 and 2.5, respectively. (e, f) TEM image of a single plate and its selected area diffraction image. All images show several prominent large NPs with many platelike triangular geometries, but with no sign of micelles bearing small NPs. See details in the text.

produces micelle templates (see Figure 11) over the whole mole fraction range, which systematically increase in the size close to the equimolar range. Thereafter, L121-rich micelles tend to break and convert into surfactant-rich "compound micelles" in the DPS-rich region (Figures 10 and 11). All micelle templates are always loaded with tiny NPs of 2–6 nm whether they are produced in the L121- or DPS-rich regions, in accordance with their origin from the surface cavities.[20−22,26,27] Likewise, L121 with TPS (C14) also leads to the formation of well-defined micelle templates of different shapes (Figures 10 and 11) loaded with tiny NPs in the L121-rich region, but they tend to deform as the mole fraction increases and eventually disappear in the TPS-rich region of the mixture with no sign of the compound micelles. Instead, large platelike triangular NPs are generated along with other polyhedral small NPs. The shape transitions become even more prominent in the case of HPS (C16) and long, rod-shaped micelles loaded with tiny NPs are formed in the L121-rich region. They are highly susceptible to shape change with a rise in the mole fraction and also carry large NPs produced from the smaller ones due to the interparticle fusion. The latter process is facilitated by the greater solubilizing[50−52] ability of HPS in view of its longer hydrocarbon tail that confines PEO–PPO surface cavities in small pockets, thus allowing tiny NPs to undergo interparticle fusion to produce larger ones. A further increase in the mole fraction only produces platelike NPs close to equimolar as well as in the HPS-rich regions.

The above results (phase diagram, Figure 10) indicate that the concentration and hydrophobicity are the most important parameters of a surfactant, which determine the self-assembled arrangement of NPs on the micellar templates. Low hydrophobicity and low concentration help in maintaining the stability of L121 micelles in the aqueous phase without disturbing very much the surface cavities. High hydrophobicity

dx.doi.org/10.1021/jp310507m | J. Phys. Chem. B 2013, 117, 3028–3039

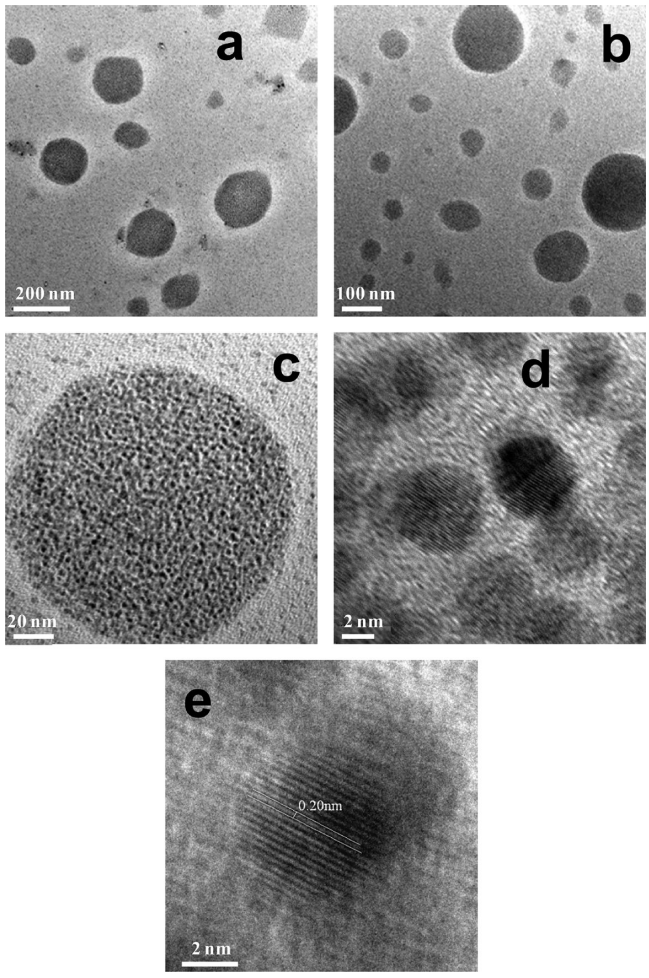

Figure 9. (a, b) Low-resolution TEM images of samples with DG/L121 and DDM/L121 mole ratio = 0.5, respectively, showing large spherical micelles loaded with tiny NPs. Panel (c) shows a single micelle, while the high-resolution image of tiny NPs is shown in (d). Panel (e) shows a single-crystal NP with lattice fringes of 0.20 nm spacing.

needs space in the core to accommodate a long hydrocarbon tail. Likewise, high concentration needs more zwitterionic head groups to be adjusted in the shell. The former facilitates the solubilization of PPO blocks in the hydrocarbon environment provided by the surfactant and hence dismantles the L121 micelles, whereas the latter disturbs the arrangement of surface cavities and reduces its reduction potential. Since the primary purpose of the surfactant is to facilitate the solubilization of otherwise insoluble L121 micelles in the aqueous phase so as to use them as templates, therefore, the concentration effect helps to achieve this over a wide range only in the case of DPS due to its low hydrophobicity. TPS and HPS cannot be used over a similar concentration range due to their much enhanced hydrophobicity; therefore, their low concentration is required to produce well-defined micelle templates.

The presence of surface cavities on micelle templates is another important factor. Without their presence, it seems quite difficult to bring and accommodate NPs on micelle templates. It should be mentioned that all NPs synthesized by the surface cavities remain self-assembled on the micelle templates and none exit independently, especially in the L121-rich region. It means that, as long as surface cavities exist, the self-assembled

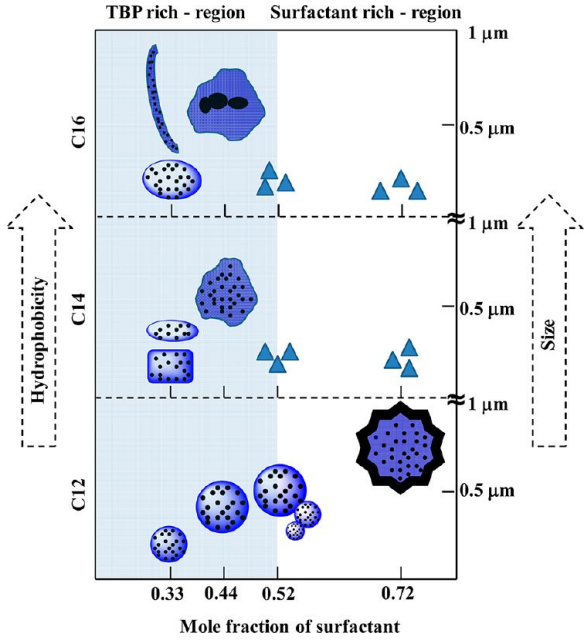

Figure 10. Proposed phase diagram showing the relationship among hydrophobicity, size of the micelles and NPs, and mole fraction of different surfactants. C12, C14, and C16 represent DPS, TPS, and HPS, respectively. Phase diagram has been divided into TBP-rich and surfactant-rich regions. See details in the text.

arrangement of NPs survives on the micelle templates. Thus, the presence of surface cavities or reducing sites on micelle templates is required to achieve a self-assembled arrangement of NPs and hence allow their direct visualization through imaging studies. Addition of gold salt in the concentration range of 0.25−1 mM is not expected to influence the overall shape and structure of the L121 micelles due to their nonionic nature. Moreover, previous studies[53,54] have demonstrated that poly(styrene)-*b*-poly(styrenesulfonate) diblock polymer micelles are not affected even up to the addition of 0.2 M NaCl, while no change in the number density of F88 TBP micelles[4] is observed up to 2 M KCl. However, PEO and PPO dehydration occurs when a high salt concentration of 1 M or more than this is used, which causes eventually shape transitions.[55] Thus, the present study is considered to provide direct visualization of L121 micelles and their shape transitions in the presence of Au NPs and can be easily extended to other predominantly hydrophobic copolymers.

■ CONCLUDING REMARKS

Micelles of water-insoluble highly hydrophobic L121 are used as templates for self-assembled NPs. L121 is made water-soluble by using small amounts of conventional surfactants. Surfactants allow the solubilization of L121 in aqueous phase, but the micelle templates are produced only in the presence of those surfactants that cause minimum disruption to L121 micelles. Concentration and hydrophobicity of neutral surfactants are the two important parameters that govern the existence of micelle templates. A low hydrophobic surfactant with a low concentration produces well-defined micelles loaded with self-assembled tiny NPs, whereas a surfactant with high hydrophobicity tends to dismantle the micelle templates by its enhanced solubilizing effects. Stability of the micelle template is the key factor to having a self-assembled arrangement of NPs because it is further related to the arrangement of surface

dx.doi.org/10.1021/jp310507m | *J. Phys. Chem. B* 2013, 117, 3028−3039

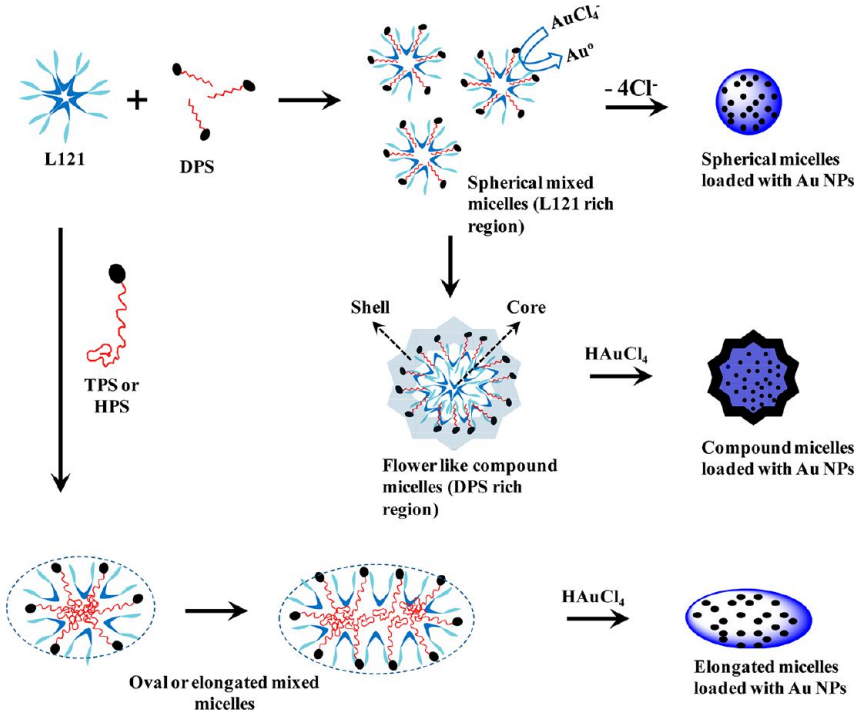

Figure 11. Schematic representation of the mixed micelle formation between L121 and zwitterionic surfactants and their subsequent use as micelle templates for the self-assembled Au NPs. Top reaction shows the formation of spherical L121 + DPS mixed micelles in the L121-rich region of the mixture by incorporating the hydrocarbon chains of DPS molecules in the L121 micelles. In the DPS-rich region, predominantly hydrophobic L121 is solubilized by the hydrocarbon tails of DPS in the form of a typical compound micelle where DPS molecules occupy the shell while L121 resides in the core, resulting in the formation of flower-like morphologies with Au NPs mainly accommodated in the core due to the presence of L121 surface cavities. Lower reaction shows that using TPS or HPS instead of DPS induces their longer hydrocarbon tails in the L121 micelles, thus causing structure transitions with the formation of oval or elongated morphologies that are visualized by the self-assembled Au NPs.

cavities, which are the reduction sites for the conversion of Au(III) into Au(0) to synthesize Au NPs. Therefore, as long as this arrangement is minimally disturbed in the presence of surfactant, NPs produced by the surface cavities remain self-assembled on the micelle templates and do not leave the micelles. Low concentration and low hydrophobicity of neutral surfactants show minimum disturbance to this arrangement and thus produce well-defined micelles loaded with tiny NPs.

■ ASSOCIATED CONTENT

Supporting Information

UV−visible spectra and TEM images. This material is available free of charge via the Internet at http://pubs.acs.org.

■ AUTHOR INFORMATION

Corresponding Author

*E-mail: ms_bakshi@yahoo.com.

Notes

The authors declare no competing financial interest.

■ ACKNOWLEDGMENTS

These studies were partially supported by financial assistance from CSIR [Ref no: 01(2683)/12], New Delhi. G.K. thankfully acknowledges the financial support provided by the Research and Development Council (RDC) of Newfoundland and Labrador, NSERC, and the Office of Applied Research at CNA.

■ REFERENCES

(1) Ghosh, S.; Dey, S.; Mandal, U.; Adhikari, A.; Mondal, S. K.; Bhattacharyya, K. Ultrafast proton transfer of pyranine in a supramolecular assembly: PEO−PPO−PEO triblock copolymer and CTAC. *J. Phys. Chem. B* **2007**, *111*, 13504−10.

(2) Dey, S.; Adhikari, A.; Mandal, U.; Ghosh, S.; Bhattacharyya, K. A femtosecond study of excitation wavelength dependence of a triblock copolymer−surfactant supramolecular assembly: $(PEO)_{20}$−$(PPO)_{70}$−$(PEO)_{20}$ and CTAC. *J. Phys. Chem. B* **2008**, *112*, 5020−5026.

(3) Liu, Y.; Chen, S. H.; Huang, J. S. Light-scattering studies of concentrated copolymer micellar solutions. *Macromolecules* **1998**, *31*, 6226−6233.

(4) Jain, N. J.; Aswal, V. K.; Goyal, P. S.; Bahadur, P. Micellar structure of an ethylene oxide−propylene oxide block copolymer: A small-angle neutron scattering study. *J. Phys. Chem. B* **1998**, *102*, 8452−8458.

(5) Alexandridis, P.; Holzwarth, J. K.; Hatton, T. A. Micellization of poly(ethylene oxide)-poly(propylene oxide)-poly(ethylene oxide) triblock copolymers in aqueous solutions: Thermodynamics of copolymer association. *Macromolecules* **1994**, *27*, 2414−2425.

(6) Bakshi, M. S.; Singh, J.; Kaur, G. Antagonistic mixing behavior of cationic gemini surfactants and triblock polymers in mixed micelles. *J. Colloid Interface Sci.* **2005**, *285*, 403−412.

(7) Bakshi, M. S.; Kaur, N.; Mahajan, R. K. A comparative behaviour of photophysical properties of Pluronic F127 and Triton X-100 with conventional zwitterionic and anionic surfactants. *J. Photochem. Photobiol., A* **2006**, *183*, 146−153.

(8) Bakshi, M. S.; Sachar, S. Influence of temperature on the mixed micelles of Pluronic F127 andP103 with dimethylene (bisdodecyldimethylammonium bromide. *J. Colloid Interface Sci.* **2006**, *296*, 309−315.

(9) Bakshi, M. S.; Sachar, S. Influence of hydrophobicity on mixed micelles of pluronic F127 and P103 plus cationic surfactants mixtures. *Colloids Surf., A* **2006**, *276*, 146−154.

(10) Bakshi, M. S.; Kaura, A.; Kaur, G. Effect of temperature on unfavourable mixing between tetraethylene glycol dodecyl ether and Pluronic 103. *J. Colloid Interface Sci.* **2006**, *296*, 370−373.

(11) Bakshi, M. S.; Bhandari, P. Fluorescence studies on the non-ideal mixing in triblock copolymer binary mixtures under the effect of temperature: A block hydration effect. *J. Photochem. Photobiol., A* **2007**, *186*, 166−172.
(12) Shimoni, K.; Danino, D. Imperfect dissolution in nonionic block copolymer and surfactant mixtures. *Langmuir* **2009**, *25*, 2736−2742.
(13) Schillen, K.; Jansson, J.; Lof, D.; Costa, T. Mixed micelles of a PEO−PPO−PEO triblock copolymer (P123) and a nonionic surfactant ($C_{12}EO_6$) in water. A dynamic and static light scattering study. *J. Phys. Chem. B* **2008**, *112*, 5551−5562.
(14) Couderc-Azouani, S.; Sidhu, J.; Thurn, T.; Xu, R.; Bloor, D. M.; Penfold, J.; Holzwarth, J. F.; Wyn-Jones, E. Binding of sodium dodecyl sulfate and hexaethylene glycol mono-*n*-dodecyl ether to the block copolymer L64: Electromotive force, microcalorimetry, surface tension, and small angle neutron scattering investigations of mixed micelles and polymer/micellar surfactant complexes. *Langmuir* **2005**, *21*, 10197−10208.
(15) Li, Y.; Xu, R.; Couderc, S.; Bloor, D. M.; Holzwarth, J. F.; Wyn-Jones, E. Binding of tetradecyltrimethylammonium bromide to the ABA block copolymer Pluronic F127 (EO_{97} PO_{69} EO_{97}): Electromotive force, microcalorimetry, and light scattering studies. *Langmuir* **2001**, *17*, 5742−5747.
(16) Jansson, J.; Schillen, K.; Olofsson, G.; Cardoso da Silva, R.; Loh, W. The Interaction between PEO−PPO−PEO triblock copolymers and ionic surfactants in aqueous solution studied using light scattering and calorimetry. *J. Phys. Chem. B* **2004**, *108*, 82−92.
(17) Lof, D.; Schillen, K.; Torres, M. F.; Muller, A. J. Rheological study of the shape transition of block copolymer−nonionic surfactant mixed micelles. *Langmuir* **2007**, *23*, 11000−11006.
(18) Cardoso da Silva, R.; Olofsson, G.; Schillén, K.; Loh, W. Influence of ionic surfactants on the aggregation of poly(ethylene oxide)−poly(propylene oxide)−poly(ethylene oxide) block copolymers studied by differential scanning and isothermal titration calorimetry. *J. Phys. Chem. B* **2002**, *106*, 1239−1246.
(19) Thurn, T.; Couderc, S.; Sidhu, J.; Bloor, D. M.; Penfold, J.; Holzwarth, J. F.; Wyn-Jones, E. Study of mixed micelles and interaction parameters for ABA triblock copolymers of the type EO_m−PO_n−EO_m and ionic surfactants: Equilibrium and structure. *Langmuir* **2002**, *18*, 9267−9275.
(20) Sakai, T.; Alexandridis, P. Mechanism of gold metal ion reduction, nanoparticle growth and size control in aqueous amphiphilic block copolymer solutions at ambient conditions. *J. Phys. Chem. B* **2005**, *109*, 7766−7777.
(21) Sakai, T.; Alexandridis, P. Spontaneous formation of gold nanoparticles in poly(ethylene oxide)−poly(propylene oxide) solutions: Solvent quality and polymer structure effects. *Langmuir* **2005**, *21*, 8019−8025.
(22) Sakai, T.; Alexandridis, P. Ag and Au monometallic and bimetallic colloids: Morphogenesis in amphiphilic block copolymer solutions. *Chem. Mater.* **2006**, *18*, 2577−2583.
(23) Sidorov, S. N.; Bronstein, L. M.; Kabachii, Y. A.; Valetsky, P. M.; Soo, P. L.; Maysinger, D.; Eisenberg, A. Influence of metalation on the morphologies of poly(ethylene oxide)-*block*-poly(4-vinylpyridine) block copolymer micelles. *Langmuir* **2004**, *20*, 3543−3550.
(24) Azzam, T.; Eisenberg, A. Monolayer-protected gold nanoparticles by the self-assembly of micellar poly(ethylene oxide)-*b*-poly(ε-caprolactone) block copolymer. *Langmuir* **2007**, *23*, 2126−2132.
(25) Mai, Y.; Eisenberg, A. A controlled incorporation of particles into the central portion of block copolymer rods and micelles. *Macromolecules* **2011**, *44*, 3179−3183.
(26) Khullar, P.; Singh, V.; Mahal, A.; Kaur, H.; Singh, V.; Banipal, T. S.; Kaur, G.; Bakshi, M. S. Tuning shape and size of gold nanoparticles with triblock polymer micelle structure transitions and environments. *J. Phys. Chem. C* **2011**, *115*, 10442−10454.
(27) Khullar, P.; Mahal, A.; Singh, V.; Banipal, T. S.; Kaur, G.; Bakshi, M. S. How PEO−PPO−PEO triblock polymer micelles control the synthesis of gold nanoparticles: Temperature and hydrophobic effects. *Langmuir* **2010**, *26*, 11363−11371.
(28) Antonietti, M.; Wenz, E.; Bronstein, L.; Seregina, M. Synthesis and characterization of noble metal colloids in block copolymer micelles. *Adv. Mater.* **1995**, *7*, 1000−1005.
(29) Moffitt, M.; McMahon, L.; Pessel, V.; Eisenberg, A. Size Control of nanoparticles in semiconductor−polymer composites. 2. Control via sizes of spherical ionic microdomains in styrene-based diblock ionomers. *Chem. Mater.* **1995**, *7*, 1185−1192.
(30) Zhao, M.; Crooks, R. M. Dendrimer-encapsulated Pt nanoparticles: Synthesis, characterization, and applications to catalysis. *Adv. Mater.* **1999**, *11*, 217−220.
(31) Bronstein, L. M. Nanoparticles made in mesoporous solids. *Top. Curr. Chem.* **2003**, *226*, 55−89.
(32) Tanori, J.; Duxin, N.; Petit, C.; Lisiecki, I.; Veillet, P.; Pileni, M. P. Synthesis of nanosize metallic and alloyed particles in ordered phases. *Colloid Polym. Sci.* **1995**, *273*, 886−892.
(33) Haes, A. J.; Stuart, D. A.; Nie, S.; Van Duyne, R. P. Using solution-phase nanoparticles, surface-confined nanoparticles array and single nanoparticles as biological sensing platforms. *J. Fluoresc.* **2004**, *14*, 355−367.
(34) Selvakannan, P. R.; Mandal, S.; Phadtare, S.; Pasricha, R.; Sastry, M. Capping of gold nanoparticles by the amino acid lysine renders them water-dispersible. *Langmuir* **2003**, *19*, 3545−3549.
(35) Hu, M.; Chen, J.; Li, Z.-Y.; Au, L.; Hartland, G. V.; Li, X.; Marquez, M.; Xia, Y. Gold nanostructures: Engineering their plasmonic properties for biomedical applications. *Chem. Soc. Rev.* **2006**, *35*, 1084−1094.
(36) Wang, M.; Kumar, S.; Lee, A.; Felorzabihi, N.; Shen, L.; Zhao, F.; Froimowicz, P.; Scholes, G. D.; Winnik, M. A. A water soluble, pH-responsive molecular brush of poly(*N*,*N*-dimethylaminoethyl methacrylate) grafted polythiophene. *J. Am. Chem. Soc.* **2008**, *130*, 9481−9491.
(37) Wang, M.; Zhang, M.; Li, J.; Kumar, S.; Walker, G. C.; Scholes, G. D.; Winnik, M. A. Self-assembly of colloidal quantum dots on the scaffold of triblock copolymer micelles. *ACS Appl. Mater. Interface* **2010**, *2*, 3160−3169.
(38) Zhang, M.; Wang, M.; He, S.; Qian, J.; Saffari, A.; Lee, A.; Kumar, S.; Hassan, Y.; Guenther, A.; Scholes, G.; Winnik, M. A. Sphere-to-wormlike network tansition of block copolymer micelles containing CdSe quantum dots in the corona. *Macromolecules* **2010**, *43*, 5066−5074.
(39) Jones, M. R.; Osberg, K. D.; Macfarlane, R. J.; Langille, M. R.; Mirkin, C. A. Templated techniques for the synthesis and assembly of plasmonic nanostructures. *Chem. Rev.* **2011**, *111*, 3736−3827.
(40) El-Sayed, M. A.; Eustis, S. Why gold nanoparticles are more precious than pretty gold: Noble metal surface plasmon resonance and its enhancement of the radiative and nonradiative properties of nanocrystals of different shapes. *Chem. Soc. Rev.* **2006**, *35*, 209−217.
(41) Liz-Marzán, L. M. Tailoring surface plasmons through the morphology and assembly of metal nanoparticles. *Langmuir* **2006**, *22*, 32−41.
(42) Kositza, M. J.; Bohne, C.; Alexandridis, P.; Hatton, T. A.; Holzwarth, J. F. Dynamics of micro- and macrophase separation of amphiphilic block-copolymers in aqueous solution. *Macromolecules* **1999**, *32*, 5539−5551.
(43) Kositza, M. J.; Bohne, C.; Alexandridis, P.; Hatton, T. A.; Holzwarth, J. F. Micellization dynamics and impurity solubilization of block copolymer L64 in an aqueous solution. *Langmuir* **1999**, *15*, 322−325.
(44) Jia, X.; Listak, J.; Witherspoon, V.; Kalu, E. E.; Yang, X.; Bockstaller, M. R. Effect of matrix molecular weight on the coarsening mechanism of polymer-grafted gold nanocrystals. *Langmuir* **2010**, *26*, 12190−12197.
(45) Bechelany, M.; Maeder, X.; Riesterer, J.; Hankache, J.; Lerose, D.; Christiansen, S.; Michler, J.; Philippe, L. Synthesis mechanisms of organized gold nanoparticles: Influence of annealing temperature and atmosphere. *Cryst. Growth Des.* **2010**, *10*, 587−596.
(46) Yu, Y.; Zhang, L.; Eisenberg, A. Morphogenic effect of solvent on crew-cut aggregates of apmphiphilic diblock copolymers. *Macromolecules* **1998**, *31*, 1144−1154.

(47) Kim, J. U.; Cha, S. H.; Shin, K.; Jho, J. Y.; Lee, J. Preparation of gold nanowires and nanosheets in bulk block copolymer phases under mild conditions. *Adv. Mater.* **2004**, *16*, 459−464.
(48) Shang, B. Z.; Wang, Z.; Larson, R. G. Effect of headgroup size, charge, and solvent structure on polymer−micelle interactions studied by molecular dynamics simulation. *J. Phys. Chem. B* **2009**, *113*, 15170−15180.
(49) Jacquin, M.; Muller, P.; Cottet, H.; Crooks, R.; Theodoly, O. Controlling the melting of kinetically frozen poly(butyl acrylate-*b*-acrylic acid) micelles via addition of surfactant. *Langmuir* **2007**, *23*, 9939−9948.
(50) Alexandridis, P.; Andersson, K. Reverse micelle formation and water solubilization by polyoxyalkylene block copolymers in organic solvent. *J. Phys. Chem. B* **1997**, *101*, 8103−8111.
(51) Todorov, P. D.; Marinov, G. S.; Kralchevsky, P. A.; Denkov, N. D.; Durbut, P.; Broze, G.; Mehreteab, A. Kinetics of Triglyceride solubilization by micellar solutions of nonionic surfactant and triblock copolymer. 3. Experiments with single drops. *Langmuir* **2002**, *18*, 7896−7905.
(52) Choucair, A.; Eisenberg, A. Interfacial solubilization of model amphiphilic molecules in block copolymer micelles. *J. Am. Chem. Soc.* **2003**, *125*, 11993−12000.
(53) Kaewsaiha, P.; Matsumoto, K.; Matsuoka, H. Sphere-to-rod transition of non-surface-active amphiphilic diblock copolymer micelles: A small-angle neutron scattering study. *Langmuir* **2007**, *23*, 9162−9169.
(54) Matsuoka, H.; Maeda, S.; Kaewsaiha, P.; Matsumoto, K. Micellization of non-surface-active diblock copolymers in water. Special characteristics of poly(styrene)-*block*-poly(styrenesulfonate). *Langmuir* **2004**, *20*, 7412−7421.
(55) Ma, J. h.; Guo, C.; Tang, Y. l.; Wang, J.; Zheng, L.; Liang, X. f.; Chen, S.; Liu, H. z. Salt-Induced micellization of a triblock copolymer in aqueous solution: A ^{1}H nuclear magnetic resonance spectroscopy study. *Langmuir* **2007**, *23*, 3075−3083.